Parasitology Research (2019) 118:935–944
https://doi.org/10.1007/s00436-018-06197-3

PROTOZOOLOGY - ORIGINAL PAPER

Micronemal protein 13 contributes to the optimal growth of *Toxoplasma gondii* under stress conditions

Shu Ye[1] · Ningbo Xia[1] · Pengfei Zhao[1] · Jichao Yang[1] · Yanqin Zhou[1] · Bang Shen[1,2] · Junlong Zhao[1,2,3]

Received: 31 August 2018 / Accepted: 28 December 2018 / Published online: 11 January 2019

Abstract

Toxoplasma gondii is a ubiquitous parasitic protozoan infecting humans and a wide variety of animals. Fast-replicating tachyzoites during acute infection and slowly growing bradyzoites during chronic infection are the two basic forms of *T. gondii* in intermediate hosts. Interconversion between the two contributes to the transmission and pathogenesis of this parasite. Secretory micronemal proteins are thought to mediate interactions with host cells and facilitate parasite invasion, therefore the majority of them are highly expressed in tachyzoites. Micronemal protein 13 (MIC13) is unique in that its expression is low in tachyzoites and is upregulated under bradyzoite-inducing conditions. Previous attempts to disrupt this gene were not successful, implying that it may play critical roles during parasite growth. However, in this study, MIC13 was successfully disrupted in type 1 strain RH and type 2 strain ME49 using CRISPR/Cas9-mediated gene disruption techniques. Consistent with its low expression in tachyzoites and increased expression under stress or bradyzoite-inducing conditions, MIC13-inactivated mutants displayed normal growth, host cell invasion, intracellular replication, and egress, as well as acute virulence at the tachyzoite stage. However, under stress conditions, such as high pH or oxygen limitation, MIC13-disrupted parasites showed significantly slower growth rates compared to the parental strains, suggesting that it is required for optimal parasite growth under bradyzoite-inducing or stress conditions. This is the first micronemal protein reported to have such expression pattern and function modes, which expands our understanding of the diverse functions of micronemal proteins.

Keywords MIC13 · Bradyzoite · Stress · *Toxoplasma gondii* · Micronemal protein

Introduction

Toxoplasma gondii is an obligate intracellular protozoan infecting humans and almost all warm-blooded animals. As an opportunistic pathogen, its infection in healthy individuals is often asymptomatic (Elmore et al. 2010). However, congenital infections may lead to abortion, stillbirth, or abnormal fetus developments in both humans and animals, leading to great economic losses and social problems (Dubey et al. 2012; Hirdes et al. 2012). In addition, people with compromised immune functions, such as AIDS patients and those on immunosuppressant medication, are at high risk of toxoplasmosis (Montoya and Liesenfeld 2004). *T. gondii* has a complicated life cycle, one unique feature is that it can be transmitted between intermediate hosts, without the involvement of definitive hosts cats. There are two forms of *T. gondii* parasites in intermediate hosts: fast-replicating tachyzoites that cause the clinical symptoms during acute infections, and slowly growing bradyzoites that are responsible for lifelong chronic infections. Depending on the environments and growth conditions, the parasites can interchange between these two forms and such interconversion plays critical roles in the pathogenesis and transmission of *T. gondii* (Lyons et al. 2002).

To some extent, bradyzoite formation can be viewed as a stress response in parasites experiencing adverse environments. In vitro, bradyzoites can be induced by a variety of

Section Editor: Dana Mordue

✉ Bang Shen
shenbang@mail.hzau.edu.cn

✉ Junlong Zhao
zhaojunlong@mail.hzau.edu.cn

[1] State Key Laboratory of Agricultural Microbiology, Huazhong Agricultural University, Wuhan, Hubei Province, People's Republic of China

[2] Key Laboratory of Preventive Medicine in Hubei Province, Wuhan, Hubei Province, People's Republic of China

[3] Hubei Cooperative Innovation Center for Sustainable Pig Production, Wuhan, Hubei Province, People's Republic of China

conditions, including extreme pH (6.6–6.8 or 8.0–8.2), high temperature (43 °C), nutrition starvation, and metabolic inhibitors (Ferreira da Silva Mda et al. 2008; Skariah et al. 2010; Soete et al. 1993). These treatments reduce the growth and slow down the cell cycle progression of the parasites, and induce the expression of bradyzoite-specific genes. In vivo, pressure from hosts' immune clearance is thought to be the primary driven force of bradyzoite formation and cyst development (Hunter and Sibley 2012), but the underlying mechanisms are largely unknown. Cysts are commonly found in brain and muscle tissues (Remington and Cavanaugh 1965). Reactivation of bradyzoites to tachyzoites occurs when the immune functions of chronically infected individuals are compromised, which can lead to severe acute toxoplasmosis, even death. A significant portion of human toxoplasmosis cases are caused by reactivation of chronic infection (Jr and Jeffers 2012). The molecular mechanisms controlling the interconversion between tachyzoites and bradyzoites are major issues to be addressed in the *T. gondii* pathogenesis research field; however, currently, very little is known. A group of transcription factors (called ApiAP2) with sequence homology to the plant APETALA2/ethylene responsive factors (AP2/ERF) are shown to be involved in the regulation of bradyzoite differentiation and cyst development (White et al. 2014). However, different ApiAP2 factors seem to have different working modes. For example AP2IX-9 and AP2IV-4 suppress the expression of bradyzoite-specific genes at the tachyzoite stage (Radke et al. 2013; Radke et al. 2018), whereas AP2XI-4 activates the expression of such genes during bradyzoite transition (Walker et al. 2013). Transcriptomic analyses using microarray and RNA-Seq techniques have identified hundreds of differentially regulated genes between tachyzoites and bradyzoites (Pittman et al. 2014). But the biological significance of these genes in the life cycle of *T. gondii* is still poorly understood.

Micronemes are unique secretory organelles in apicomplexan parasites, which include *T. gondii*. The majority of proteins stored in and secreted by micronemes are involved in various steps of host cell invasion (Carruthers and Boothroyd 2007; Frénal et al. 2017). Apical membrane antigen 1 (AMA1), the most extensively studied micronemal protein, mediates moving junction formation along with rhoptry neck protein 2 (RON2) to initiate invasion (Bargieri et al. 2013; Krishnamurthy et al. 2016). A handful of micronemal proteins (MICs) contain adhesive motifs, such as chitin binding-like (CBL), microneme adhesive repeat (MAR), and thrombospondin like domains, to facilitate host cell interactions. MICs often contain transmembrane (TM) domains or glycosylphosphatidylinositol (GPI) anchors to allow surface localization after being released from micronemes (Carruthers and Tomley 2008). But there are exceptions, MIC1 and MIC3 do not have TM motifs or GPI modification; instead, they form complexes with MIC4/MIC6 and MIC8 respectively to achieve surface localization (Brecht et al. 2001; Matthias et al. 2001; Meissner et al. 2002). Both adhesive motifs and surface exposure are critical for the proper function of MICs during parasite invasion.

Due to their roles in promoting parasite invasion, expressions of the majority of MICs peak at the tachyzoite stage. However, in analyzing the gene expression datasets deposited in ToxoDB, we found that expression of MIC13 was very different than other MICs. It was significantly upregulated during chronic infection in vivo, and during stress-induced bradyzoite formation in vitro. MIC13 contains microneme adhesive repeat (MAR) domains to recognize and bind sialic acids on host cell surface. It does not contain TM motifs or GPI anchors. Previous attempts to knock out MIC13 in RH or Δ*ku80* strains were not successful, implying that it played critical roles and was refractory to inactivation (Friedrich et al. 2010). Nonetheless, using the most recent CRISPR/Cas9-mediated gene editing techniques, we successfully disrupted *MIC13* in both type 1 and type 2 strains. Phenotypic analysis suggested that it did not play significant roles in tachyzoite invasion or growth; instead, it contributed to optimal parasite growth under stress conditions.

Material and methods

Experimental animals, parasite strains, and growth conditions

Seven-week-old female ICR mice were purchased from the Center of Disease Control and Prevention in Hubei Province, and were maintained under standard conditions according to the regulations specified by Administration of Affairs Concerning Experimental Animals. All animal experiments were approved by the Ethical Committee of Huazhong Agricultural University (permit no. HZAUMO-2017-023).

All genetically modified strains used in this study were generated from the parental strains ME49 or RH Δ*hxgprt* (RH), which were maintained by growth in human foreskin fibroblast (HFF) cells (purchased from ATCC, Manassas, VA, USA) cultured in Dulbecco's modified Eagle medium (DMEM) supplemented with 2% fetal bovine serum (Life Technologies, Inc., Rockville, MD, USA), 10 U/ml penicillin and 100 μg/ml streptomycin. Tachyzoites of other strains were grown in the same way.

Plasmids construction

All primers used in this study are listed in Table 1. The MIC13 targeting CRISPR plasmid was constructed by replacing the UPRT targeting guide RNA (gRNA) in pSAG1::CAS9-U6::sgUPRT (Addgene #54467) with a MIC13 targeting gRNA by site-directed mutagenesis, as described previously

Table 1 Primer used in this study

Primer	Sequence	Used for
gRNA-MIC13-Fw	5′-CGCAACGCATGCGTCATGGCGTTTTAGAGCTAGAAATAGC	To construct the MIC13-specific CRISPR plasmid
gRNA-Rv	5′-AACTTGACATCCCCATTTAC	To construct gene-specific CRISPR plasmids
DHFR-Fw	5′-CAGGCTGTAAATCCCGTGAG	Amplification of DHFR fragment
DHFR-Rv	5′-GATTCCGTCAGCGGTCTGTC	Amplification of DHFR fragment
U5MIC13-Fw	5′-CCCGCGCATCTTGCCACTGA	Amplification of 5′-homology of MIC13 for 5H-DHFR*-3H construction
U5MIC13-Rv	5′-CTCACGGGATTTACAGCCTGCAAAGTTGTGCTTTCATGAC	Amplification of 5′-homology of MIC13 for 5H-DHFR*-3H construction
U3MIC13-Fw	5′-GACAGACCGCTGACGGAATCCTCAACTACTTGACAGTCCG	Amplification of 3′-homology of MIC13 for 5H-DHFR*-3H construction
U3MIC13-Rv	5′-CACACTACGCACAGTATCGA	Amplification of 3′-homology of MIC13 for 5H-DHFR*-3H construction
5′-UpU5MIC13	5′-GGCAGCCACGACACAGAAAG	PCR1 of Δ*mic13*
3′-InDHFR	5′-CAAGACGCAGACGCATACAA	PCR1 of Δ*mic13*
5′-InDHFR	5′-CGCACGGACGAATCCAGATG	PCR2 of Δ*mic13*
3′-DnU3MIC13	5′-GTTCCAGAAGCCATGTGATC	PCR2 of Δ*mic13*
In-MIC13-Fw	5′-TCACGTACGAGGCTAGATCC	PCR3 of Δ*mic13*
In-MIC13-Rw	5′-GACTTCCATCTGTTCGACAG	PCR3 of Δ*mic13*
RT-tubulin-Fw	5′-CACTGGTACACGGGTGAAGGT	β-tubulin-based qPCR
RT-tubulin-Rv	5′-ATTCTCCCTCTTCCTCTGCG	β-tubulin-based qPCR
RT-MIC13-Fw	5′-AACTGCGGCGGTGAAATA	MIC13-based qPCR
RT-MIC13-Rv	5′-GCAAATTGGTGGGTTGATGG	MIC13-based qPCR

(Shen et al. 2014). To generate the 5H-DHFR-3H homologous templates for replacing *MIC13* with the selectable markers *DHFR*-TS*, 5′- and 3′-homologous arms of MIC13 were amplified from genomic DNA of RH Δ*hxgprt* strain and the DHFR mini gene cassette was amplified from the plasmid pUPRT-DHFR-D (Shen et al. 2014). Subsequently, these fragments were then ligated together by overlapping PCR to generate 5H-DHFR-3H, which was used as template in further PCR amplifications (use U5MIC13-Fw and U3MIC13-Rv as primers, Table 1) to obtain enough amount of homologous templates for transfection. Plasmid and homologous templates were sequenced before use.

MIC13 inactivation mutants construction

To make the *MIC13* deletion mutant in RH, 7.5 μg *MIC13* targeting CRISPR/Cas9 plasmid and 1.5 μg homologous template (5H-DHFR-3H) were co-transfected into RH *Δhxgprt*, selected with 1 μM pyrimethamine and single cloned by limiting dilution in 96-well plates seeded with HFF monolayers. To disrupt *MIC13* in ME49 by insertional mutagenesis, 7.5 μg *MIC13* targeting CRISPR/Cas9 plasmid and 1.5 μg selectable markers DHFR*-TS (amplified from pUPRT-DHFR-D) were transfected into freshly egressed ME49, selected and single cloned as above. Single clones were identified by diagnostic PCRs, and the expression of MIC13 in these mutants was further examined by qRT-PCR.

Plaque assay

Freshly egressed tachyzoites were purified by filtration through 3.0-μm polycarbonate membranes and counted with a hemocytometer under a Nikon Eclipse TS100 phase contrast microscope (Nikon Instruments, Tokyo, Japan). Subsequently, parasites were inoculated into six-well plates (200 tachyzoites/well) seeded with confluent HFF monolayers, and allowed to grow for 8 (RH strains) or 12 days (ME49 strain days) without disturbance at 37 °C with 5% CO_2. Then the samples were fixed with 4% paraformaldehyde and stained with 1% crystal violet. Plaques were imaged with a scanner and the numbers and sizes of plaques were analyzed as previously described (Shen and Sibley 2014).

Virulence tests in mice

Freshly egressed tachyzoites were purified and used to infect 7-week-old female ICR mice (10 mice/strain, 100 tachyzoites/mouse) by intraperitoneal injection. Then the symptoms were recorded daily and the mice were euthanized when signs indicative of irreversible death were first observed. Cumulative mortality was graphed as Kaplan-Meier survival plots and

analyzed in Prism 5 (GraphPad Software Inc., La Jolla, CA, USA).

Invasion assay

Freshly egressed parasites were purified by a 3-μm membrane filtration, counted, and then used to infect HFF monolayers seeded on coverslips (5×10^6 tachyzoites per coverslip in 24-well plates) for 20 min at 37 °C. Subsequently, the coverslips were quickly washed with PBS and fixed with paraformaldehyde for immunofluorescent analysis. Invaded (extracelluar) vs non-invaded (intracellular) parasites were distinguished by a two-color staining protocol described previously (Huynh et al. 2003). Extracellular parasites were stained with swine anti-Toxo and total parasites were stained with rabbit anti-TgALD. Primary antibodies were detected by FITC-conjugated goat anti-swine IgG and Alexa 594-conjugated goat anti-rabbit IgG secondary antibodies (Life Technologies, Inc., Rockville, MD, USA). Samples were then analyzed by fluorescent microscopy, using a BX53 Olympus microscope (Olympus Life Science, Tokyo, Japan). Invasion efficiency was determined as: number of invaded parasites divided by the number of hose cell nuclei. The invasion efficiency of the parental strains was artificially set as 100% and corresponding mutants were normalized accordingly.

Intracellular replication assay

Parasites pretreated with standard tachyzoite growth conditions for 2 days, or bradyzoite-inducing (pH = 8.2, ambient CO_2) conditions for 4 days, or 3% oxygen for 3 days, were purified and used to infect HFF monolayers seeded on coverslips (Xia et al. 2018). After 1-h invasion, extracellular parasites were washed away with phosphate buffered saline (PBS). The invaded parasites were cultured for another 24–36 h under the corresponding pretreatment conditions. Then the samples were fixed for immune fluorescence analysis as described in the above "Invasion assay" section. The parasitophorous vacuoles (PVs) that were stained red only were included for analysis. PVs containing 1, 2, 4, 8, 16, or more parasites were counted and analyzed. At least 200 PVs were examined for each strain in each experiment, and each strain was tested three times independently.

Induced egress

Confluent HFF monolayers seeded on coverslips in 24-well plates were infected with 10^6/well purified tachyzoites and cultured at 37 °C for 32 h. Then extracellular parasites were washed away with PBS. Intracellular parasites were then treated with 1% DMSO or 2 μM calcium ionophore A23187 (Shanghai Aladdin Biochemical Technology Co., Ltd., Shanghai, China) at 37 °C for 2 min (Daher et al. 2010). Samples were fixed and stained with mouse TgSAG1 monoclonal antibody DG52 (a gift from Dr. David Sibley at Washington University in St Louis), followed by Alexa 488-conjugated goat anti-mouse IgG secondary antibody to visualize the integrity of PVs. The number of both egressed and intact vacuoles was counted, and egress efficiency was determined by dividing the number of egressed vacuoles by the number of total vacuoles. Each strain was tested three times independently.

Bradyzoite differentiation

Tachyzoites were allowed to infect HFF cells in T25 flasks and cultured under bradyzoite-inducing conditions (alkaline media with pH = 8.2, ambient CO_2) for 4 days (Ueno et al. 2009). The induced parasites were then allowed to infect confluent HFF monolayers and induced for another 3 days. Subsequently, the samples were subject to immunofluorescent analysis. Bradyzoites were stained with mouse anti-TgBAG1 and all parasites were stained with rabbit anti-TgALD. Bradyzoite differentiation was determined by dividing the number of $TgBAG1^+$ vacuoles by that of $TgALD^+$ vacuoles. The experiments were repeated three times independently.

Quantitative real-time PCR

Freshly egressed tachyzoites or alkaline-induced bradyzoites (10^7 per sample) were purified and collected for RNA isolation using the trizol methods (TransGen Biotech, China). Subsequently, 2 μg total RNA of each sample was reverse transcribed into cDNA using the PrimeScript RT reagent Kit (Takara Bio, Japan), according to the manufacturer's instructions. Then quantitative real-time PCR was performed to check the MIC13 transcript levels in each sample, using the SYBR Green method on the ViiA-7 Real-Time system (Life Technologies, Rockville, MD, USA). Expression of the β-tubulin was used as an internal reference (Selseleh et al. 2012).

Statistical analysis

Statistical analyses were performed in Prism 5(GraphPad Software Inc., La Jolla, CA, USA) using Student's *t* tests or two-way analysis of variance, as indicated in figure legends.

Results

Domain structure and expression pattern of *T. gondii* MIC13

Available gene expression data suggests that most micronemal proteins are well expressed in tachyzoites and do not show obvious changes during interconversion between tachyzoites

and stress-induced bradyzoites in vitro (Fig. 1a, data from ToxoDB). TgMIC13 is unique in that its expression is relatively low in tachyzoites and is significantly upregulated in bradyzoites induced in vitro (Fig. 1a). This was also true in vivo, expression of TgMIC13 was found to be much higher at chronic infection stage than acute infection stage (the Pittman RNA-Seq dataset in ToxoDB). To further confirm the expression patterns of TgMIC13, total RNA isolated from tachyzoites and alkaline (medium with pH = 8.2, ambient CO_2)-induced bradyzoites was reverse transcribed and subject to quantitative RT-PCR analysis. Using β-tubulin as an internal reference, the results showed that alkaline induction led to over 30-fold increase in TgMIC13 expression (Fig. 1b). Taken together, these results suggested that TgMIC13 expression was increased under stress or bradyzoite-inducing conditions.

Consistent with TgMIC13 being a secretory micronemal protein, it has a signal peptide (Fig. 1c), as predicted by the program SignalP 4.1. Homology-based sequence analysis suggested that TgMIC13 contained three MAR (micronemal adhesive repeat) domains with sialic-acid binding activities (Fig. 1c). In addition, proteins with significant similarities to TgMIC13 can be found in other coccidian parasites, including *Neospora caninum*, *Hammondia hammondi*, and *Cystoisospora suis* (Fig. 1d), indicating a conserved role of MIC13 in this group of parasites.

Disruption of MIC13 in type 1 and type 2 *T. gondii* strains

To study the biological functions of MIC13 in *T. gondii*, it was disrupted in type 1 strain RH and type 2 strain ME49 by two different strategies. TgMIC13 was completely knocked out in RH by CRISPR/CAS9-mediated homologous gene replacement with the pyrimethamine-resistant marker *DHFR** (Fig. 2a). After co-transfecting the MIC13 targeting CRISPR plasmid and the homology template (5H-DHFR*-3H) into RH Δ*hxgprt*, transfectants were selected with pyrimethamine and single clones were obtained by limiting dilution. Diagnostic PCRs were used to examine the disruption of MIC13 (Fig. 2a). TgMIC13 null mutants were easily obtained and diagnostic PCRs on one such clone were shown in Fig. 2b: the presence of a 1387-bp PCR1 product and a 1662-bp PCR2 product indicated the correct integration of *DHFR** into the *TgMIC13* locus. The absence of a 1020-bp PCR3 product derived from the *TgMIC13* gene further confirmed the complete disruption of this gene (Fig. 2b). In

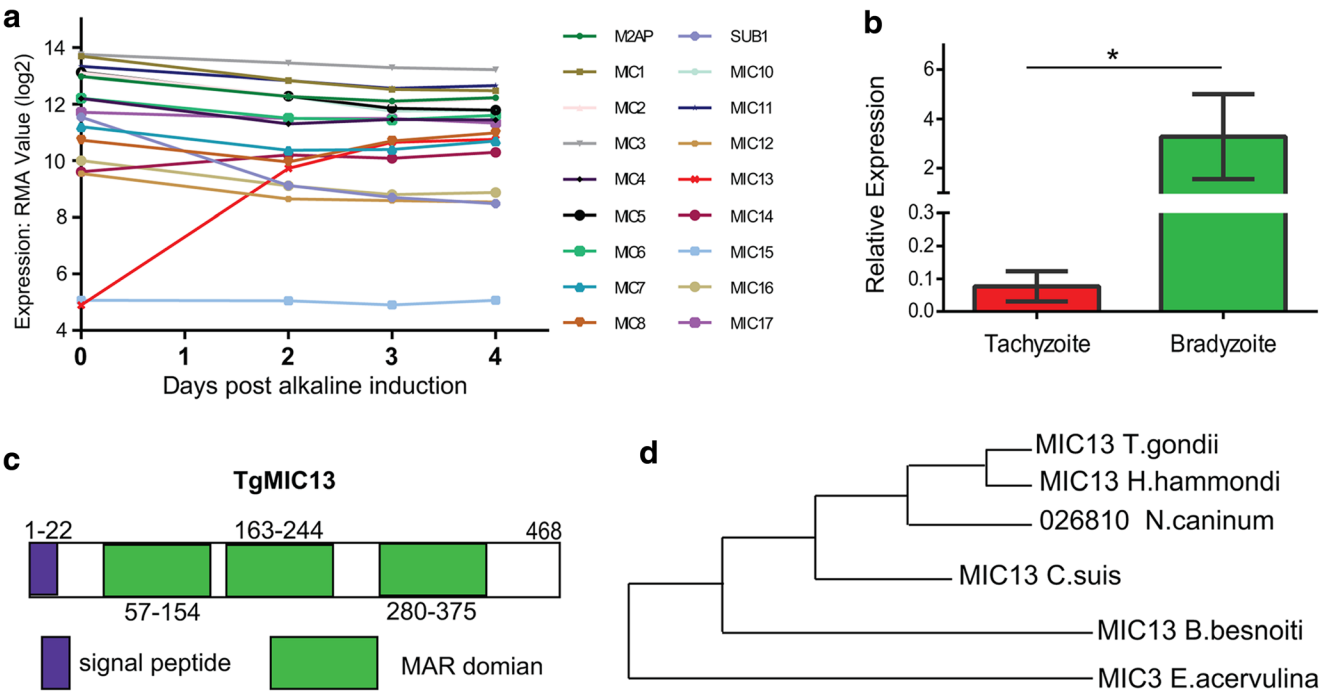

Fig. 1 Expression and Domain structure of TgMIC13. **a** Expression changes of selected micronemal proteins during alkaline-induced bradyzoite differentiation in vitro. Microarray gene expression profiles deposited in ToxoDB (dataset: bradyzoite differentiation (3-day time series)) were used to generate the graph. **b** Relative expression levels of *TgMIC13* in *Toxoplasma* tachyzoites and alkaline-induced bradyzoites in vitro. Parasites were collected to extract total RNA which was reverse transcribed into cDNA later. Using β-tubulin as an internal reference, quantitative real-time PCR was used to estimate the transcript levels for *TgMIC13* in each sample. Data from four independent experiments, $*p < 0.05$, Student's *t* test. **c** Domain structure of TgMIC13 predicted by Motifscan using the PFAM database, which suggest that it has three MAR (micronemal adhesive repeat) domains with sialic acid binding activities. The numbers indicate the amino acid positions. **d** Phylogenetic relationship between TgMIC13 and related proteins from other parasites. Protein sequences were subject to BLAST search on NCBI and the tree was constructed by Mega

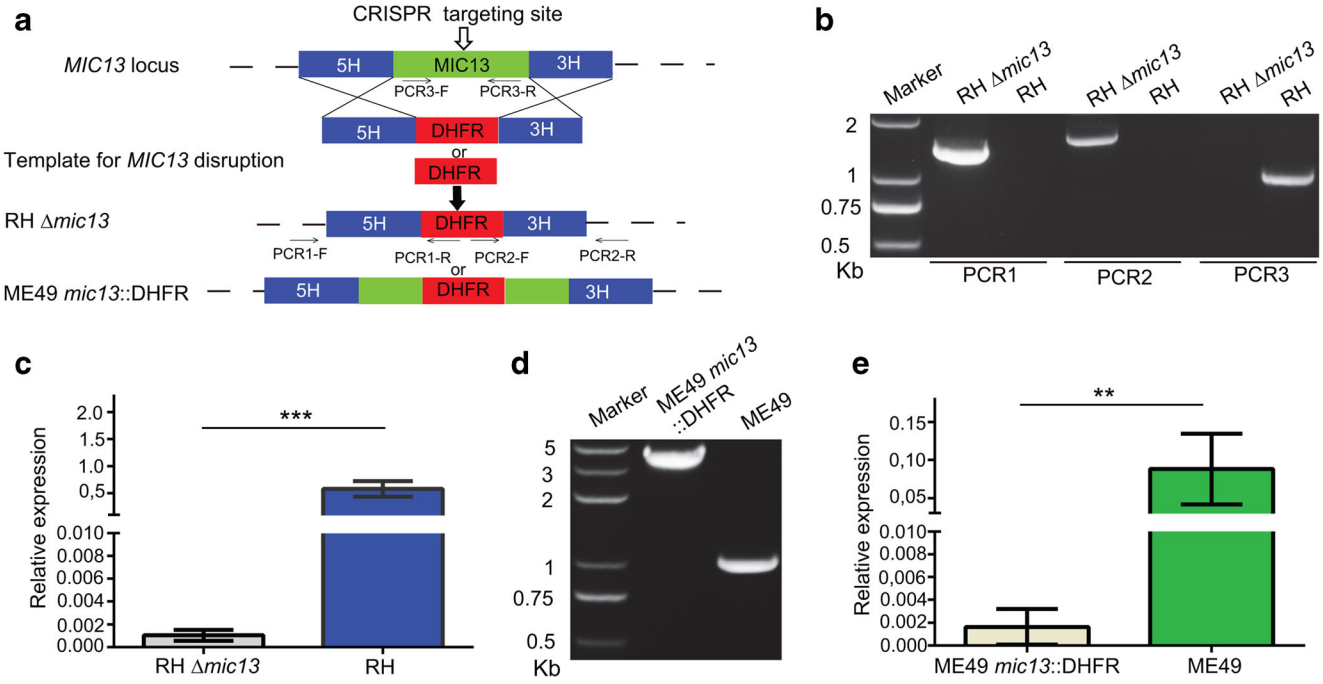

Fig. 2 Generation of *TgMIC13* disruption mutants. **a** Schematic illustration of *TgMIC13* disruption by CRISPR/CAS9-mediated homologous gene replacement in RH or site-specific insertion of *DHFR* selectable cassette insertion in ME49. PCR1/PCR2/PCR3-F/R denotes the primer designs of diagnostic PCRs used in (**b**) and (**d**). PCR1 and PCR2 check the 5′ and 3′ integration of the selection marker, whereas PCR3 examines the integrity of the *TgMIC13* gene. The open arrow indicates the CRISPR/Cas9 targeting site. (**b**) and (**d**) Diagnostic PCRs for *TgMIC13* disruption mutants in RH and ME49 respectively. (**c**) and (**e**) RT-PCR examining the transcript levels of *TgMIC13* in tachyzoites of indicated strains, as done in Fig. 1B. ***$p < 0.0001$, **$p < 0$ .001, Student's *t* test

addition, quantitative RT-PCR analysis using total RNA extracted from RH *Δmic13* suggested that the expression of MIC13 in the mutant was below the detection limit of RT-PCR (Fig. 2c), further supporting the loss of *MIC13* in the mutant.

Inactivation of TgMIC13 in type 2 strain ME49 was achieved by inserting the selection marker DHFR* into the fourth exon of TgMIC13 genomic sequence, by CRISPR/CAS9-mediated site-specific insertion (Fig. 2a). The presence of a 4.3-kb PCR3 product suggested the correct insertion of *DHFR** into TgMIC13 (Fig. 2d), whereas the same PCR on wild-type strains produced a 1020-bp product. Similarly, quantitative RT-PCR analysis also confirmed the loss of *TgMIC13* expression in the insertional mutant (Fig. 2e). Successful disruption of *TgMIC13* in both RH and ME49 strains suggested that this gene was not required for parasite growth, which indicated that previous failures in inactivating this gene were likely due to technical issues.

Characterization of the growth of *TgMIC13* inactivation mutants in vitro

Although *TgMIC13* was not essential in the parasites, we still wanted to test whether it contributed to parasite growth at all. To do that, plaque assay was performed to assess the overall fitness of the *TgMIC13* mutants. After 8 days of growth in confluent HFF monolayers, RH *Δmic13* produced very similar number of plaques as the parental strain RH (Fig. 3a). In addition, when the sizes of plaques were analyzed, there were no noticeable differences between the mutant and the wild-type strain either (Fig. 3b). Same results were also observed in ME49 strains after 12 days of plaque development, ME49 *Δmic13* produced similar number and size of plaques as the parental strain ME49 (Fig. 3a, b). Together, these results suggested that TgMIC13 played very little role in parasite growth in vitro.

To further check the impact of TgMIC13 on parasite fitness, we compared the invasion, intracellular replication, and egress efficiencies of the *TgMIC13* mutants to that of wild-type parasites, using ME49 strains grown under standard growth conditions. Over a 15-min invasion course, tachyzoites of the ME49 *Δmic13* displayed very similar invasion efficiency as ME49 (Fig. 4a), suggesting that TgMIC13 was not required for tachyzoite invasion. Intracellular replication assays were performed to assess the contribution of TgMIC13 to parasite replication under standard growth conditions in vitro. After successful invasion, parasites were allowed to replicate in HFF cells for 24 h, a time point when more than half of the PVs of the ME49 strain contained 8 or more tachyzoites (Fig. 4b). The size distribution of PVs in the ME49 *Δmic13* mutant was very similar to that of the parental ME49 strain, suggesting that TgMIC13 did not have an active role in parasite replication

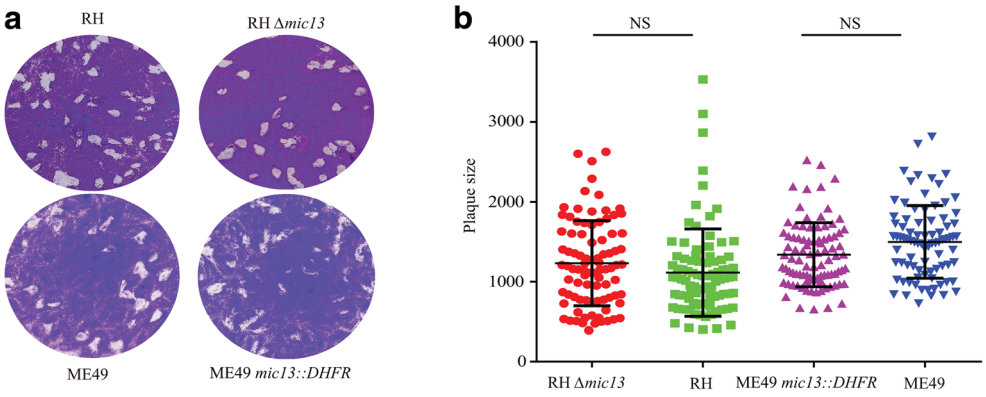

Fig. 3 Normal growth of *TgMIC13*-deficient mutants in vitro. **a** Plaque assay comparing the growth of *TgMIC13* mutants to that of the parental strains in vitro. **b** Relative size of plaques in Fig. 3a. A minimum of 85 plaques was analyzed for each strain

under these settings. To test the egress efficiency, tachyzoites were grown until the majority of PVs containing 16 or more parasites. Then egress was artificially induced by the addition of calcium ionophore A23187 and egress was monitored by checking the integrity of PVs. As shown in Fig. 4c, A23187 induction led to egress of over 90% of the PVs in both ME49 and ME49 *Δmic13* (Fig. 4c), indicating that TgMIC13 was not required for tachyzoite egress either.

Virulence of *TgMIC13* mutants in mice

To evaluate the acute virulence of *Δmic13* mutants in vivo, they were used to infect ICR mice by intraperitoneal injection. Corresponding parental strains were included as controls and the survival of mice was monitored daily after infection. Mice infected with RH showed signs of irreversible death within 8 days and RH *Δmic13*–infected mice displayed similar survival kinetics (Fig. 5a). Same is true for ME49 strains, ME49 *Δmic13* showed almost the same virulence as the parental ME49 (Fig. 5b). Together, these results suggested that TgMIC13 does not contribute to parasite virulence in mice.

TgMIC13 is required for optimal parasite growth under stress conditions

As mentioned above, expression of *TgMIC13* was significantly increased upon stress treatments or bradyzoite induction, indicating that it may have a role during adaptation to these environments. To test this possibility, intracellular replication assay was used to estimate the replication efficiency of two independent *Δmic13* mutants under stress conditions. Parasites were first pretreated with bradyzoite-inducing conditions (culture medium with pH = 8.2, CO_2 starvation with ambient CO_2 supply) for 4 days and then used to infect HFF cells and grown for another 36 h under the same conditions. Subsequently, the replication of parasites was determined by checking the number of parasites in PVs. As shown in Fig. 6a, in the case of ME49, the PV population was dominated by the ones containing 2, 4 or 8 parasites. However, for the two *Δmic13* mutants, the majority of PVs harbored only 1, 2 or 4 parasites (Fig. 6a), suggesting that the replication of *Δmic13* mutants was slower than that of the wild-type strain under stress conditions. One possible reason for the slower growth is higher bradyzoite transition. To test whether this is the case

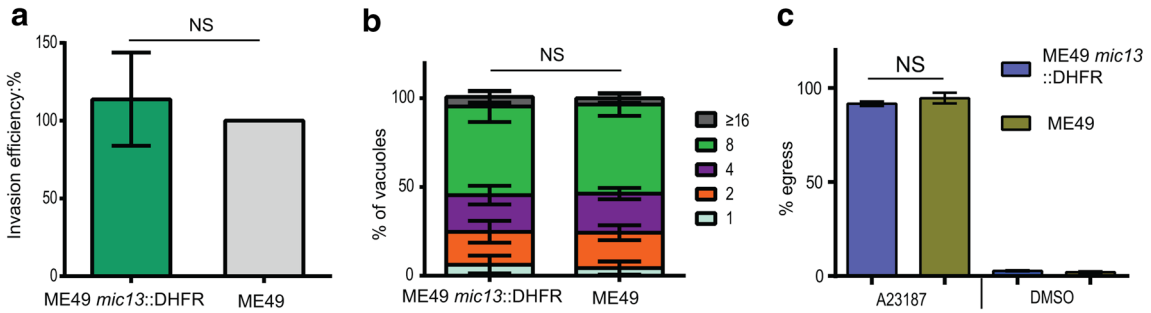

Fig. 4 Invasion, intracellular replication, and egress of *MIC13*-deficient tachyzoites in vitro. **a** Freshly egressed tachyzoites were used to invade HFF cells for 15 min. Then a two-color staining approach was used to distinguish invaded vs non-invaded parasites, to estimate the invasion efficiency. The invasion efficiency of the parental strain ME49 was artificially set as 100% and that of the mutant was compared to this reference. NS, not significant; Student's *t* test. **b** Purified tachyzoites were used to infect HFF monolayers for 15 min and invaded parasites were allowed to replicate for 24 h. Subsequently, the numbers of vacuoles containing 1, 2, 4, 8, or 16 parasites were counted. At least 200 vacuoles were analyzed for each strain, each with three independent experiments. NS, not significant; two-way ANOVA. **c** Egress efficiency of *TgMIC13*-disrupted mutants. 32-h post infection of host cells by the parasites, 3 μmol ionophore A23187 was added into culture medium to induce parasite egress. After 5 min of induction, samples were fixed with 4% formaldehyde and the integrity of PV was determined by phase contrast microscopy. Disrupted PV indicated successful egress. NS, not significant; Student's *t* tests

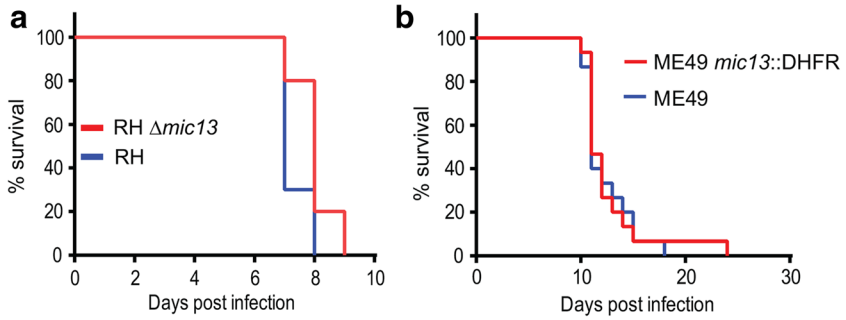

Fig. 5 Acute virulence of *MIC13* mutants in mice. *TgMIC13*-deficient mutants, as well as the corresponding parental strains, were used to infect ICR mice (100 tachyzoites per mouse, 10 mice for each strain) by intraperitoneal injection, and the survival of mice was monitored daily. (**a**) and (**b**) Survival curves of mice infected with RH Δ*mic13* and ME49 *mic13::DHFR*, respectively

for ME49 *Δmic13*, similarly treated parasites were stained for the expression of the bradyzoite-specific marker BAG1, to estimate bradyzoite formation efficiency. The results showed that ME49 *Δmic13* actually displayed slightly lower rates of bradyzoite transition (Fig. 6b), indicating that slower growth of ME49 *Δmic13* under stress conditions is not due to increased bradyzoite transition. We also used oxygen restriction (3%) as a stress condition to test the growth of ME49 *Δmic13*. The results showed that oxygen limitation also led to reduced replication in the *Δmic13* mutant (Fig. 6c). Collectively, these results indicate that MIC13 is required for the optimal growth of *T. gondii* under stress conditions, which is consistent with its increased expression after stress treatments.

Discussion

Unlike most other micronemal proteins that are well expressed in the tachyzoite stage to facilitate parasite infection of host cells, expression of *TgMIC13* is relatively low in tachyzoites but is increased significantly in bradyzoites or under stress conditions. Previous attempts to knock out *TgMIC13* were not successful, implying that it might have critical roles for parasite growth (Friedrich et al. 2010). In this study, *TgMIC13* was disrupted in both type 1 and type 2 *T. gondii* strains to assess its functions during parasite growth and development. Consistent with its expression pattern, *TgMIC13* did not seem to play any role in tachyzoite invasion, replication, or egress, nor did it contribute to acute virulence in mice. Instead, it was found to be required for the optimal growth of parasites under stress or bradyzoite-inducing conditions. The successful inactivation of TgMIC13 suggested that previous failures in *TgMIC13* knockout were likely due to technical challenges.

A handful of micronemal proteins are extensively studied to be involved in parasite invasion of host cells (Cérède et al. 2005; Huynh and Carruthers 2006; Kessler et al. 2008). Many

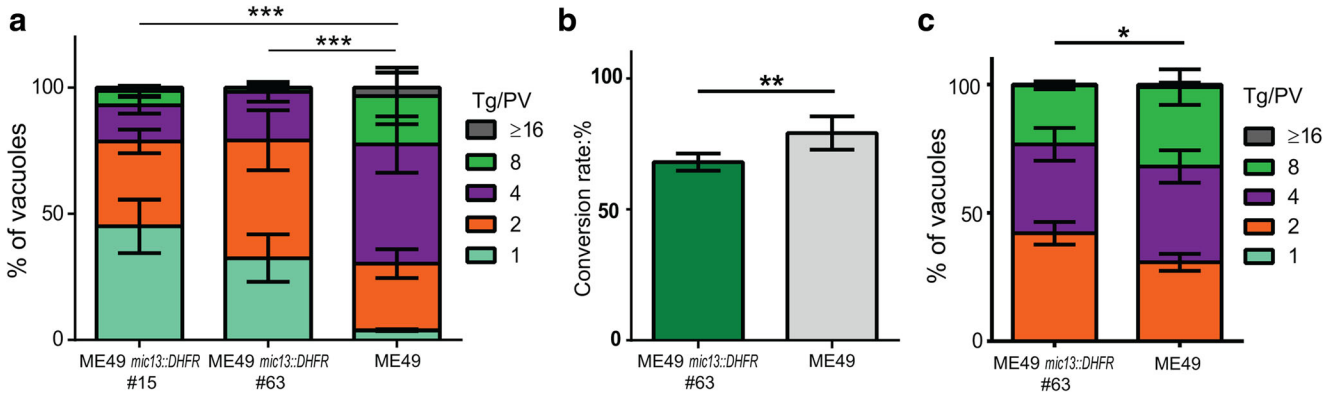

Fig. 6 Decreased replication of *MIC13*-deficient mutants under stress conditions. **a** Intracellular replication assay of parasites under bradyzoite-inducing conditions. WT and two independent *mic13::DHF* mutants were first treated by alkaline (pH = 8.2, ambient CO_2) growth conditions for 4 days; subsequently, they were used to infect HFF cells and grown for another 36 h under the same alkaline conditions. Parasite replication was determined as in Fig. 4b. ***$p < 0.0001$, two-way ANOVA. **b** Bradyzoites conversion assay. Parasites were induced to bradyzoites with the above alkaline media for 7 days. Subsequently, the samples were fixed and stained with goat anti-ALD (to stain total parasites) and mouse anti-BAG1 (to stain bradyzoites). Conversion rates were calculated by the number of $BAG1^+$ vacuoles by that of ALD^+ vacuoles. **$p < 0$ .01, Student's *t* tests with three independent experiments. (**c**) Intracellular replication under 3% oxygen. Parasites were cultured with 3% oxygen for 3 days and then used to infect HFF monolayers. After 24-h growth under 3% oxygen, parasite replication was determined in the same way as Fig. 4b. *$p < 0.05$, two-way ANOVA

of these proteins contain adhesive domains such as intergrin A–like domains, PAN/apple domains, and galectin-like domains, to mediate protein-protein and protein-carbohydrates interactions (Carruthers and Tomley 2008). TgMIC13 is similar to these micronemal proteins in that it also contains adhesive motifs. Sequence analysis indicated that it contained three microneme adhesive repeat (MAR) domains with sialic acid binding activities. MARs are also found in other micronemal proteins such as MIC1, which is able to form complex with MIC4 and MIC6 and bind to host cell surface (Brecht et al. 2001; Matthias et al. 2001). MIC1 plays important roles during parasite invasion and the binding of its MAR domains to sialylated glycoconjugates contributes to efficient invasion (Blumenschein et al. 2007; Friedrich et al. 2010). Nevertheless, although MIC13 contains three MARs, it does not seem to contribute to parasite invasion. MIC13-disrupted mutants had normal invasion efficiencies as the parental strains. In addition, sequence analysis did not predict the presence of transmembrane domain or glycosylphosphatidylinositol motif in TgMIC13 (Friedrich et al. 2010). Therefore, unless it forms complex with other surface-anchored proteins, it is not able to localize to parasite surface. This may be another reason why TgMIC13 functions differently than other micronemal proteins.

Our quantitative RT-PCR analysis, as well as existing gene expression data generated by others, all showed that expression of TgMIC13 was increased under stress or bradyzoite-inducing conditions (Fritz et al. 2012). This is unusual for a micronemal protein and in fact is the only micronemal protein known so far to have such expression pattern. Upregulation of TgMIC13 expression under stress conditions suggests that it might have a role in this process. Indeed, the *TgMIC13* knockout strain displayed slower replication than wild-type parasites if treated with alkaline medium in combination with CO_2 starvation or oxygen limitation. The slower growth of the *Δmic13* mutants under these conditions was not due to increased bradyzoite transition; therefore, the underlying mechanisms are still to be determined. We also tried to estimate whether TgMIC13 contributed to bradyzoite formation in vivo in the mouse infection model; however, all infected mice eventually died before reliable cyst counting can be done, even with ME49 strains. Therefore, to test this role of TgMIC13, corresponding mutants may need to be made in even lower virulent strains, such as type 3 strains.

In conclusion, our study showed that expression of the micronemal protein TgMIC13 was upregulated during stress and bradyzoite-inducing conditions. Using mutants lacking *MIC13*, it was found that TgMIC13 was not required for parasite growth or invasion under standard tachyzoite growth conditions. However, it contributed to the optimal growth of parasites under stress conditions. This is the first micronemal protein described so far with such expression and function patterns.

Funding information This work was supported the National Key Research and Development Program of China (Grant no. 2017YFD0500402), the National Basic Science Research Program (973 program) of China (Grant no. 2015CB150300), and the Natural Science Foundation of Hubei Province (Project 2017CFA020). The funders had no role in the study design, data collection and analysis, preparation of the manuscript, or decision to submit the work for publication.

Compliance with ethical standards

All animal experiments were approved by the Ethical Committee of Huazhong Agricultural University (permit no. HZAUMO-2017-023).

Competing interests The authors declare they have no conflict of interest.

References

Bargieri DY, Andenmatten N, Lagal V, Thiberge S, Whitelaw JA, Tardieux I, Meissner M, Ménard R (2013) Apical membrane antigen 1 mediates apicomplexan parasite attachment but is dispensable for host cell invasion. Nat Commun 4:2552

Blumenschein TM et al (2007) Atomic resolution insight into host cell recognition by toxoplasma gondii. EMBO J 26:2808–2820

Brecht S, Carruthers VB, Ferguson DJP, Giddings OK, Wang G, Jäkle U, Harper JM, Sibley LD, Soldati D (2001) The toxoplasma micronemal protein MIC4 is an adhesin composed of six conserved apple domains. J Biol Chem 276:4119–4127

Carruthers V, Boothroyd JC (2007) Pulling together: an integrated model of Toxoplasma cell invasion. Curr Opin Microbiol 10:83–89

Carruthers VB, Tomley FM (2008) Microneme Proteins in Apicomplexans. In: Microneme proteins in apicomplexans. Springer, New York

Cérède O, Dubremetz JF, Soête M, Deslée D, Vial H, Bout D, Lebrun M (2005) Synergistic role of micronemal proteins in Toxoplasma gondii virulence. J Exp Med 201:453–463

Daher W, Plattner F, Carlier MF, Soldatifavre D (2010) Concerted action of two formins in gliding motility and host cell invasion by Toxoplasma gondii. PLoS Pathog 6:e1001132

Dubey JP, Hill DE, Rozeboom DW, Rajendran C, Choudhary S, Ferreira LR, Kwok OCH, Su C (2012) High prevalence and genotypes of Toxoplasma gondii isolated from organic pigs in northern USA. Vet Parasitol 188:14–18

Elmore SA, Jones JL, Conrad PA, Patton S, Lindsay DS, Dubey JP (2010) Toxoplasma gondii: epidemiology, feline clinical aspects, and prevention. Trends Parasitol 26:190–196. https://doi.org/10.1016/j.pt.2010.01.009

Ferreira da Silva Mda F, Barbosa HS, Gross U, Luder CG (2008) Stress-related and spontaneous stage differentiation of toxoplasma gondii. Mol BioSyst 4:824–834. https://doi.org/10.1039/b800520f

Frénal K, Dubremetz JF, Lebrun M, Soldatifavre D (2017) Gliding motility powers invasion and egress in Apicomplexa. Nat Rev Microbiol 15:645–660

Friedrich N, Santos JM, Liu Y, Palma AS, Leon E, Saouros S, Kiso M, Blackman MJ, Matthews S, Feizi T, Soldati-Favre D (2010) Members of a novel protein family containing microneme adhesive repeat domains act as sialic acid-binding lectins during host cell invasion by apicomplexan parasites. J Biol Chem 285:2064–2076

Fritz HM, Buchholz KR, Chen X, Durbinjohnson B, Rocke DM, Conrad PA, Boothroyd JC (2012) Transcriptomic analysis of toxoplasma development reveals many novel functions and structures specific to sporozoites and oocysts. PLoS One 7:e29998

Hirdes W, Davis DW, Eisenlohr BN (2012) Prevalence and genotypes of Toxoplasma gondii in pork from retail meat stores in Eastern China. Int J Food Microbiol 157:393

Hunter CA, Sibley LD (2012) Modulation of innate immunity by Toxoplasma gondii virulence effectors. Nat Rev Microbiol 10: 766–778

Huynh MH, Carruthers VB (2006) Toxoplasma MIC2 is a major determinant of invasion and virulence. PLoS Pathog 2:e84

Huynh MH, Rabenau KE, Harper JM, Beatty WL, Sibley LD, Carruthers VB (2003) Rapid invasion of host cells by Toxoplasma requires secretion of the MIC2-M2AP adhesive protein complex. EMBO J 22:2082–2090

Jr SW, Jeffers V (2012) Mechanisms of Toxoplasma gondii persistence and latency. FEMS Microbiol Rev 36:717–733

Kessler H, Herm-Götz A, Hegge S, Rauch M, Soldati-Favre D, Frischknecht F, Meissner M (2008) Microneme protein 8–a new essential invasion factor in Toxoplasma gondii. J Cell Sci 121: 947–956

Krishnamurthy S, Deng B, del Rio R, Buchholz KR, Treeck M, Urban S, Boothroyd J, Lam YW, Ward GE (2016) Not a simple tether: binding of toxoplasma gondii AMA1 to RON2 during invasion protects AMA1 from rhomboid-mediated cleavage and leads to dephosphorylation of its cytosolic tail. mBio 7(5):e00754-16

Lyons RE, Mcleod R, Roberts CW (2002) Toxoplasma gondii tachyzoite-bradyzoite interconversion. Trends Parasitol 18:198–201

Matthias R et al (2001) Identification and characterization of an escorter for two secretory adhesins in Toxoplasma gondii. J Cell Biol 152: 563–578

Meissner M, Reiss M, Viebig N, Carruthers VB, Toursel C, Tomavo S, Ajioka JW, Soldati D (2002) A family of transmembrane microneme proteins of Toxoplasma gondii contain EGF-like domains and function as escorters. J Cell Sci 115:563–574

Montoya JG, Liesenfeld O (2004) Toxoplasmosis. Lancet 363:1965–1976

Pittman KJ, Aliota MT, Knoll LJ (2014) Dual transcriptional profiling of mice and Toxoplasma gondii during acute and chronic infection. BMC Genomics 15(1(2014-09-20) 15):806

Radke JB, Lucas O, de Silva EK, Ma Y, Sullivan WJ Jr, Weiss LM, Llinas M, White MW (2013) ApiAP2 transcription factor restricts development of the Toxoplasma tissue cyst. Proc Natl Acad Sci U S A 110:6871–6876

Radke JB, Worth D, Hong D (2018) Transcriptional repression by ApiAP2 factors is central to chronic toxoplasmosis. PLoS Pathog 14:e1007035. https://doi.org/10.1371/journal.ppat.1007035

Remington JS, Cavanaugh EN (1965) Isolation of the encysted form of Toxoplasma gondii from human skeletal muscle and brain. N Engl J Med 273:1308–1310

Selseleh M, Modarressi MH, Mohebali M, Shojaee S, Eshragian MR, Selseleh M, Azizi E, Keshavarz H (2012) Real-time RT-PCR on SAG1 and BAG1 gene expression during stage conversion in immunosuppressed mice infected with Toxoplasma gondii Tehran strain. Korean J Parasitol 50:199–205

Shen B, Sibley LD (2014) Toxoplasma aldolase is required for metabolism but dispensable for host-cell invasion. Proc Natl Acad Sci U S A 111:3567–3572. https://doi.org/10.1073/pnas.1315156111

Shen B, Brown KM, Lee TD, Sibley LD (2014) Efficient gene disruption in diverse strains of Toxoplasma gondii using CRISPR/CAS9. Mbio 5:01114–01114

Skariah S, McIntyre MK, Mordue DG (2010) Toxoplasma gondii: determinants of tachyzoite to bradyzoite conversion. Parasitol Res 107: 253–260. https://doi.org/10.1007/s00436-010-1899-6

Soete M, Fortier B, Camus D, Dubremetz JF (1993) Toxoplasma gondii: kinetics of bradyzoite-tachyzoite interconversion in vitro. Exp Parasitol 76:259–264. https://doi.org/10.1006/expr.1993.1031

Ueno A, Dautu G, Munyaka B, Carmen G, Kobayashi Y, Igarashi M (2009) Toxoplasma gondii : identification and characterization of bradyzoite-specific deoxyribose phosphate aldolase-like gene (Tg DPA). Exp Parasitol 121:55–63

Walker R, Gissot M, Croken MM, Huot L, Hot D, Kim K, Tomavo S (2013) The Toxoplasma nuclear factor TgAP2XI-4 controls bradyzoite gene expression and cyst formation. Mol Microbiol 87: 641–655

White MW, Radke JR, Radke JB (2014) Toxoplasma development - turn the switch on or off? Cell Microbiol 16:466–472

Xia N, Yang J, Ye S, Zhang L, Zhou Y, Zhao J, David Sibley L, Shen B (2018) Functional analysis of Toxoplasma lactate dehydrogenases suggests critical roles of lactate fermentation for parasite growth in vivo. Cell Microbiol 20:e12794